



OPEN

Coherent phonon optics in a chip with an electrically controlled active device

SUBJECT AREAS:
NANOSCALE DEVICES
SEMICONDUCTORS
ACOUSTICS

Caroline L. Poyser, Andrey V. Akimov, Richard P. Campion & Anthony J. Kent

School of Physics and Astronomy, University of Nottingham, Nottingham NG7 2RD, United Kingdom.

Received
12 October 2014

Accepted
6 January 2015

Published
5 February 2015

Correspondence and
requests for materials
should be addressed to
C.L.P. (ppxcp@
nottingham.ac.uk)

Phonon optics concerns operations with high-frequency acoustic waves in solid media in a similar way to how traditional optics operates with the light beams (i.e. photons). Phonon optics experiments with coherent terahertz and sub-terahertz phonons promise a revolution in various technical applications related to high-frequency acoustics, imaging, and heat transport. Previously, phonon optics used passive methods for manipulations with propagating phonon beams that did not enable their external control. Here we fabricate a phononic chip, which includes a generator of coherent monochromatic phonons with frequency 378 GHz, a sensitive coherent phonon detector, and an active layer: a doped semiconductor superlattice, with electrical contacts, inserted into the phonon propagation path. In the experiments, we demonstrate the modulation of the coherent phonon flux by an external electrical bias applied to the active layer. Phonon optics using external control broadens the spectrum of prospective applications of phononics on the nanometer scale.

Extensive experimental studies of terahertz (THz) and sub-THz coherent phonons have extended ultrasonic techniques to ever higher frequencies and become the basis for a change-of-paradigm methodology in various areas including high-frequency electronics^{1,2}, information technology^{3,4}, biosciences^{5,6}, and medical diagnostics⁷. Sub-THz phonons are the quanta of acoustic waves having nanometer wavelength, and thus it is possible to reduce the size of acoustic (i.e. phononic) devices, improve spatial resolution of acoustic imaging techniques and increase the speed of acousto-electronic and acousto-optical devices by several orders of magnitude relative to traditional ultrasonics operating at MHz frequencies. Probing nano-objects with coherent sub-THz phonons is an emerging technique, but has already shown its prospective in specific applications such as: hypersonic probing and imaging of nanostructures^{8–13} including biological cells^{5,6,14,15}; control of optical^{16,17}, magnetic^{18,19} and microwave-frequency electron transport^{1,2,20} devices. The typical high-frequency phononic circuits include nanometer phonon generators and detectors fabricated on the same chip, where coherent phonons propagate on macroscopic distances²¹. The ability to manipulate phonon beams and explore “*phonon optics*”, as previously has been achieved for photons, could lead to a revolution in development of new acoustic imaging techniques and methods to control electronic, optical, microwave, quantum and thermal devices which exploit the interaction of phonons with charges, spins and photons²².

In the two decades leading up to the 1980s, there was an intensive activity in performing phonon optic experiments²³ using incoherent acoustic phonons, e.g. heat pulses²⁴ and quasi monochromatic phonons generated and detected using superconducting tunnel junctions²⁵. These works have contributed significantly to the understanding of fundamental properties of THz phonons, including: anharmonic decay and phonon-phonon interactions; phonon scattering on impurities and defects; and interaction of phonons with other excitations (electrons, photons, magnons etc.)²⁶. Phonon optics experiments with coherent sub-THz and THz phonons started later²⁷ and showed immediately the prospective for practical applications by extending ultrasonic imaging techniques towards high frequencies and high spatial resolution^{28–32}. However, methods to control the coherent phonon beams propagating between the phonon generator and detector are limited to “passive” methods (e.g. transmission or reflection of phonons at the single³³ or multiple interfaces³⁴). The ability to control the intensity and the phase of the propagating coherent phonon beams by external means, e.g. by applying an electric field, would be a significant step towards practical applications of sub-THz phonon optics. The present work is concentrated on this challenging task.

In the present work we perform phonon optics experiments on a phononic chip which includes superlattices (SLs): a periodic array of nanometer layers with different acoustic impedances. SLs are widely used for the generation and detection of coherent phonons in phonon optics experiments; they may be made with semiconductors³⁵, metals³⁶ and soft matter³⁷. Furthermore, a doped semiconductor SL under electrical bias turns out to be an *active device* showing a phonon lasing (sasing)³⁸ effect and amplification of coherent phonons passing



through the biased SL³⁹ under appropriate conditions. However, most previous experiments with sub-THz active SLs used bolometric detection of phonons^{40,41}. This technique, although quite sensitive to the intensity of the phonon flux, does not provide information about the phonon spectrum and phase. Recently, however, we have developed a novel, extremely sensitive, detector for coherent phonons based on a *p-i-n* photodiode device⁴². The high sensitivity and THz bandwidth of this detector have enabled the present work, which is to study a phononic chip including an active SL controlled by external electrical bias. We therefore realize a novel phonon optics experimental setup that integrates, on a single semiconductor chip, a coherent phonon source, a detector of coherent phonons and an active device for electrical manipulation of the phonon beam as it makes its way from the source to the detector. We show that applying electrical bias to the doped SL, the active device, changes the amplitude and phase of the transmitted coherent phonons thus demonstrating the possibility of manipulating the phonon beam intensity with external electrical control.

The paper is organized as follows: after describing the phononic chip used in the experiment, we shall present the results of phonon generation and detection with an unbiased device, which is equivalent to a passive phononic chip. Further, we shall turn to the main experimental result of the work where we study the effect of electrical bias in the doped SL on the amplitude of the transmitted coherent phonon signal. Finally, we present analysis of the results, discussion and conclusions. The experiment and analysis details may be found in the Methods section.

Results

The design of the phononic chip and the scheme of the experiment used in the present work is shown in Fig. 1a. The chip consists of three main elements: (i) an undoped GaAs/AlAs transducer SL, in this SL coherent monochromatic phonons with a frequency $f_0 = 378$ GHz are excited by optical pulses from a femtosecond pulsed laser; (ii) an active n-doped GaAs/AlAs SL with heavily n-doped contacts for applying electrical bias; and (iii) a *p-i-n* detector of coherent phonons on the opposite side of the GaAs substrate to the SLs⁴². The SLs and *p-i-n* on both sides of the substrate were fabricated in the form of mesas (Fig. 1b) with the diameters 400 and 200 μm respectively, centred exactly opposite to each other. The contact pattern on the devices was designed to allow optical accesses for generation of coherent phonons in the transducer SL and probing the phonon beam in *p-i-n* detector. The low temperature current-voltage (*I-V*) characteristic of the active SL device is shown in Fig. 1c. It is linear up to an applied bias of about 500 mV in the negative direction and 800 mV in the positive direction, whereupon oscillations appear due to the formation of space charge domains in the SL⁴³. More details concerning the sample fabrication are presented in the Methods section.

In experiments with the phononic chip the generated phonons pass through the active SL, where the bias V is applied, then through the GaAs substrate with thickness of $d = 164$ μm , and finally are detected using optical probing with temporal resolution ~ 1 ps in the *p-i-n* detector. The detected signal $P_V(t)$ is monitored as function of the delay t between pump and probe pulses. The $P_V(t)$ provides direct information about the temporal evolution of dynamical strain in the *p-i-n* which accompanies the coherent acoustic wavepacket. The techniques for generation and detection of coherent phonons are well developed so won't be discussed in detail here, details of the current experiment may be found in the Methods section and earlier papers describing generation in a SL⁴⁴ and detection by a *p-i-n* photodiode⁴². The experiments were performed at the temperature $T_0 = 10$ K to minimise attenuation of the 380 GHz phonons as they propagate through the substrate. The low temperature is also a requirement for the operation of the active SL, and ensures that the thermal broadening of the electronic energy states is no more than the energy of the

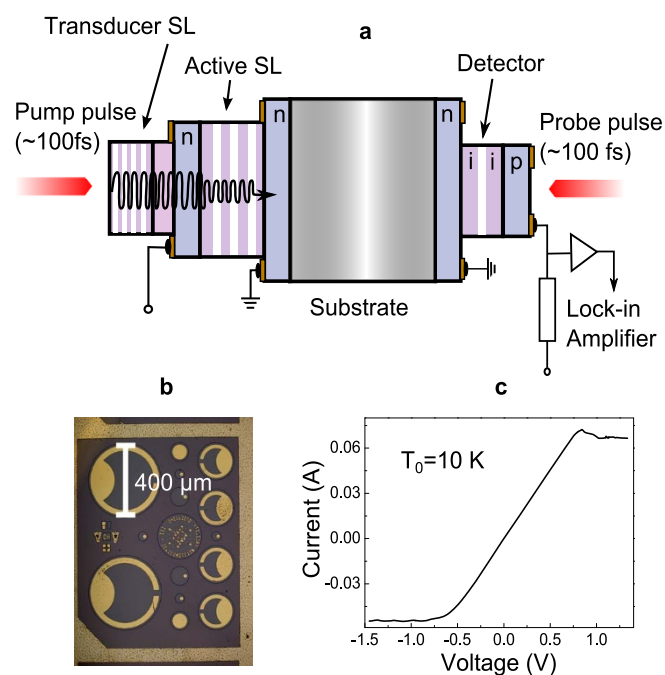


Figure 1 | Phononic chip: (a) Coherent monochromatic phonons with $f_0 = 387$ GHz are generated in the transducer SL when it is excited by optical pump pulses from the femtosecond laser. Phonons pass through the active SL where a bias V may be applied, propagate through the 164 μm thick GaAs substrate and are detected in the *p-i-n* diode with femtosecond resolution by means of optical probing from the same laser. (b) A photograph of the phononic chip from the side of the *p-i-n* photodiode. (c) The current-voltage (*I-V*) characteristic of the active SL measured at $T_0 = 10$ K.

378 GHz phonons. In our experiment the wavelength of pump and probe pulses was chosen in the range 690–700 nm to have sufficient absorption by electron-hole (exciton) optical transition in 4 nm GaAs layers and full transparency in 11 nm AlAs barriers which form the transducer SL. Then theoretical estimations predict the generation of quasi-monochromatic acoustic phonons in the transducer SL with the frequency 380 GHz and the duration of the wavepacket ~ 4 ns⁴⁴.

Active SL unbiased. With no bias applied to the active SL, the experimental device can be considered to be a passive phononic chip. The temporal evolution of the strain $P_0(t)$ detected in the *p-i-n* for the case when the bias is not applied to the active SL ($V = 0$) is shown in Fig. 2a. The temporal trace $P_0(t)$ is spread over the time interval ~ 1 ns and includes several high-amplitude peaks and harmonic oscillations with a frequency of $f_0 = 378$ GHz (see the zoomed fragment in Fig. 2a). The value $t = 0$ is defined as the arrival time of the phonons generated at the open surface of the top SL to the *p-i-n* detector after their ballistic propagation through the semiconductor chip with the average velocity 4.8 km/s (this path is shown by an arrow t_0 in the lower inset of Fig. 2a). The fast Fourier transform (FFT) of $P_0(t)$ obtained for the full temporal interval is shown in Fig. 2b. The amplitude FFT spectrum consists of a large number of closely located spikes and two well isolated peaks at $f_0 = 378$ GHz and $f_1 = 519$ GHz with the widths 2 and 10 GHz respectively indicated in Fig. 2b by the vertical arrows. The temporal shape of $P_0(t)$ and its spectrum are in agreement with the earlier results in phonon optics experiments with passive SL devices^{21,45}. The most important feature is the existence of the essential contribution from monochromatic phonons with the frequency $f_0 = 378$ GHz that is attributed to coherent phonon generation in the transducer SL as a result of pump optical excitation.

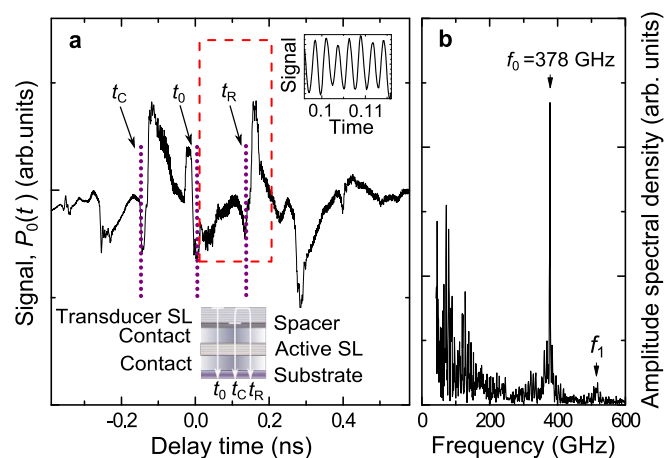


Figure 2 | Phonon optics with passive phononic chip. (a) Temporal evolution of the detected signal which accompanies the coherent phonon wavepacket in the *p-i-n* detector for $V = 0$. Sharp peaks, marked by dotted lines, correspond to the strain pulses generated at various interfaces in the phononic chip (the lower inset shows the paths corresponding to the three high amplitude peaks labeled t_0 , t_c , and t_r). The signal possesses harmonic oscillations with $f_0 = 378$ GHz (see the zoomed fragment on the upper inset). The dashed rectangle indicates the time interval where harmonic oscillations have maximum amplitude. (b) Fast Fourier Transform of the signal shown in (a) obtained in full time window from -0.3 ns up to 0.5 ns. The sharp peaks and f_0 and f_1 correspond to the coherent monochromatic phonons generated by optical pump pulses in the transducer and active SLs respectively.

A small fraction of the optical pump beam is transmitted through the contact GaAs layers and reaches the second SL where phonons with $f_1 = 519$ GHz are generated in the same way as in the top SL. High-amplitude peaks, which form the low frequency part ($f < 250$ GHz) of the phonon spectrum are due to optically induced stress in various semiconductor layers. Particularly, the peaks in $P_0(t)$ with the highest amplitudes correspond to the strain pulses generated in the heavily doped *n*-contact near the interface with the transducer SL. The arrival times t_c and t_r of the direct and reflected strain pulses respectively are shown by dotted vertical lines in Fig. 2a and the inset shows the corresponding propagation paths. More details may be found in the Methods section. The spiky character of the whole spectrum is the result of the phonon interference due to multiple reflections at the interfaces and surfaces of the phononic chip.

Further we shall concentrate on the monochromatic part of the phonon spectrum at $f_0 = 378$ GHz. The pump light penetrates into the top SL and generates coherent phonons throughout its full thickness, and so the first phonons to reach the detector will be emitted from near the bottom of the SL. As the SL is a total of 750 nm in thickness, these phonons arrive 130 ps earlier than those from the top surface. Therefore, the oscillations with frequency f_0 in $P_0(t)$ start at ≈ -130 ps. These oscillations last for a time longer than 1 ns and possess the highest amplitude in the time interval $t = 100 - 200$ ps marked by dashed rectangle. This interval will be the subject for further studies of the effect of electrical bias in the active SL on the phonon signal at $f_0 = 378$ GHz.

Active SL under bias. To study the effect of applying an electrical bias, V , to the doped SL on the coherent phonon signal $P_V(t)$ we modulate bias voltage V and detect the difference $\Delta P(t) = P_V(t) - P_0(t)$ using a digital lock-in amplifier. The frequency of the bias modulation was set at 15 kHz, which corresponds to the period much shorter than the thermal time constant of the sample, thus avoiding a significant lattice temperature modulation in the chip. This was confirmed by measuring the arrival time of the acoustic

wavepacket with bias on and off as is further explained in the discussion section. We present the results in the time interval marked by dashed frame in Fig. 2a where bias induced effects are the strongest. The measured signals $\Delta P(t)$ for $V = 500$ mV and $P_0(t)$ are shown in Fig. 3a. It is seen that both signals, $\Delta P(t)$ and $P_0(t)$, possess temporal evolutions which show oscillatory behaviour. The maximum relative changes $\Delta P(t)/P_0(t) \sim 0.14\%$ in the spectral amplitudes at f_0 are high enough to detect the signal in the phononic chip using the *p-i-n* photodiode with sufficient signal to noise level. It is important that the temporal shape of $\Delta P(t)$ is not exactly the same as the temporal shape of $P_0(t)$, which means that the origin of $\Delta P(t)$ is not simply due to a modulation of the *p-i-n* detector sensitivity by any stray electric field from the biased SL.

The FFT spectra of $P_0(t)$ and $\Delta P(t)$ are shown in Fig. 3b. The two spectra possess some similar features: both consist of the broad low frequency part and the narrow spectral line at $f_0 = 378$ GHz. The similarity between these two spectra means that the applied bias has an effect on both parts of the spectra: broadband low-frequency part ($f \leq 200$ GHz) and monochromatic coherent phonons with $f_0 = 378$ GHz. As mentioned earlier, the major contribution to the broadband low frequency part of the coherent phonon spectrum comes from the strain pulses generated in the *n*-GaAs contact where bias is applied. It is reasonable to assume that the application of bias

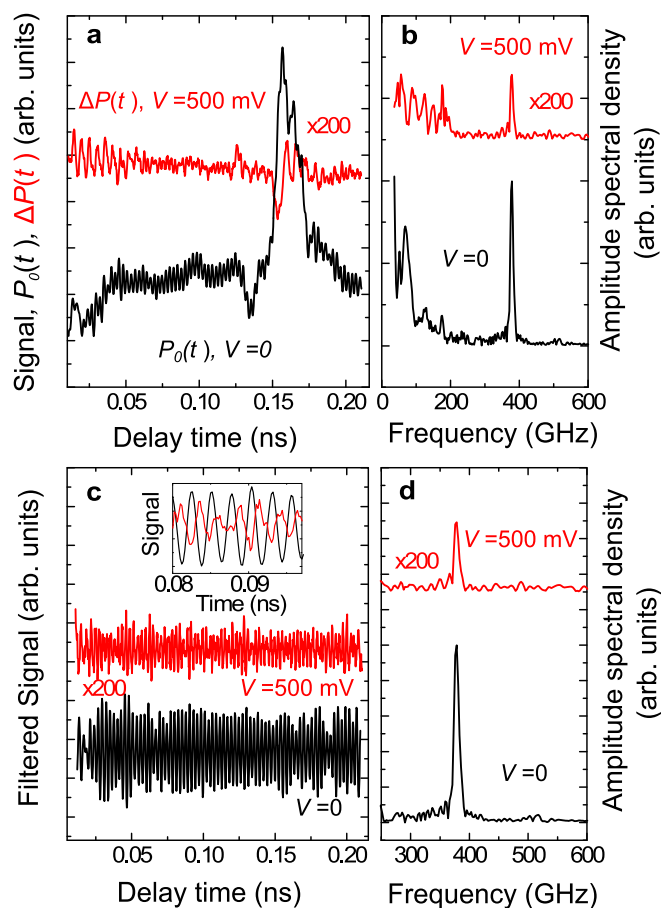


Figure 3 | Phonon optics with active phononic chip. (a) Temporal evolution of the bias modulated (modulation amplitude $V = 500$ mV) signal, $\Delta P(t)$ (red line) and the signal $P_0(t)$ (black line) measured in passive chip ($V = 0$). (b) Fast Fourier Transforms of the signals shown in (a). (c) and (d) The same as (a) and (b) respectively after applying a digital high pass filtering with the cutoff 250 GHz. The inset in (c) shows the zoomed fragments of the filtered signals, so that the phase difference $\Delta\Psi$ for harmonic oscillations at $f_0 = 378$ GHz between $\Delta P(t)$ (red line) and $P_0(t)$ (black line) is clearly seen.



changes the widths of the depletion regions in the contacts, which affects the optical absorption length and correspondingly the spectrum of the generated coherent phonons in the acoustic wavepacket of the strain pulse. This effect, while being interesting by itself, however stays beyond the present work, and further we shall concentrate on the contribution from monochromatic phonons with $f_0 = 378$ GHz to $\Delta P(t)$. The only source of these monochromatic phonons in the studied phononic chip is the transducer SL excited by the optical pump pulses.

For clarity of the presentation we apply high-pass digital filtering to $P_0(t)$ and $\Delta P(t)$ transmitted phonon spectra components with cut off frequency at 250 GHz, and show corresponding traces and spectra in Figs. 3c and 3d respectively. It is seen that after filtering the harmonic oscillations with $f_0 = 378$ GHz look more distinct and it is possible to compare the phases of the monochromatic contributions in $P_0(t)$ and $\Delta P(t)$ (see inset in Fig. 3c). Fitting the temporal curves with a harmonic function $\sim \sin(2\pi f_0 t + \Psi)$ it is possible to obtain the phase difference $\Delta\Psi = \Psi_0 - \Psi_\Delta$ where Ψ_0 and Ψ_Δ are the phases of the f_0 harmonic component $P_0(t)$ and $\Delta P(t)$ respectively. Performing the fitting procedure in seven 20 ps temporal intervals we get a value of $\Delta\Psi = (0.76 \pm 0.03)\pi$ which will be discussed in more detail in the next section.

Discussion

We start the discussion by considering the relative amplitude and phase of f_0 components in the signals $P_0(t)$ and $\Delta P(t)$. Ignoring any nonlinear effects it is easy to show that the amplitude ratio $\alpha = D/A_0$ (A_0 and D are the amplitudes of the $P_0(t)$ and $\Delta P(t)$ respectively) depends on the bias induced changes of $\Delta A = A_V - A_0$ (A_V is the amplitude of $P_V(t)$) and on the difference Δt between the arrival times of coherent phonons to the p - i - n detector with bias on and off. From the experiment we estimate $\alpha \sim 0.14\%$ for $V = \pm 500$ mV and, using the analysis described in the methods section, we deduce that $|\Delta A/A_0| \sim 0.1\%$ and $\Delta t \sim 0.4$ fs. These results show the extremely high sensitivity of the modulation technique and p - i - n phonon detection used in this experiment.

The non-zero value of Δt is most likely to be due to the bias induced modulation of the sound velocity as a result of lattice temperature modulation. Indeed, application of bias to the active SL is accompanied by Joule heat and respectively by an increase of the lattice temperature in the propagation path for phonons from the transducer SL to the p - i - n detector. From the difference in the arrival time of the phonon induced signal at $V = 0$ and 0.5 V applied bias, we estimate the average sample temperature T_1 based on the dependence of the sound velocity c on T in GaAs, i.e. $c(T) = \sqrt{c_{11}(T)/\rho(T)}$, where c_{11} and ρ are the elastic constant and density of GaAs respectively. Using the published temperature dependencies of c_{11} ⁴⁶ and ρ ⁴⁷, we estimate that the average sample temperature is raised from $T_0 = 10$ K to the value $T_1 \approx 23$ K by applying the bias.

Modulation of bias with a frequency of 15 kHz leads to modulation of the sample temperature with the amplitude ΔT , which, for the case when the modulation period is much less than the thermal time constant of the sample, is ($\ll T_1$). Assuming the measured value of the delay $\Delta t = 0.4$ fs is purely due to the temperature modulation, then using the value $\left(\frac{dc(T)}{dT}\right)_{T=T_1}$, we can estimate $\Delta T \sim 10^{-3}$ K.

Such a small value of ΔT cannot explain the measured value $|\Delta A/A_0|$ if the transmission change was due to anharmonic phonon-phonon scattering. Indeed, estimates based on Herring mechanism of anharmonic decay⁴⁸ give relative changes of the f_0 phonon amplitude of not more than 4×10^{-5} which is two orders of magnitude smaller than the experimentally measured $|\Delta A/A_0| \sim 1 \times 10^{-3}$. Thus we exclude the modulation of the lattice temperature as the reason for the bias induced modulation of the phonon flux amplitude.

Our explanation of the bias-induced modulation of the coherent phonon flux with $f_0 = 378$ GHz is based on the model of electron-

phonon interactions in the active SL. The band diagram of the SL with applied bias, where electrons are well separated in energy and space, is called a Stark ladder⁴⁹. The electrons are mostly confined within the GaAs layers, but are able to tunnel via the ALAs barriers giving rise to electrical conduction in the direction perpendicular to the SL layers. Electron transitions between states can occur with the absorption or emission of phonons within a GaAs layer, or between neighbouring GaAs layers, respectively known as intra- and inter-quantum well (QW) transitions. The coherent phonons generated and detected in the chip propagate almost exactly along the direction normal to the active SL layers. In this direction intra-QW transitions are effectively cut off for phonons of frequency 378 GHz due to the momentum conservation condition⁵⁰. The two possible phonon-induced inter-QW transitions involve stimulated absorption and stimulated emission, as illustrated in the inset of Fig. 4⁵¹. Although the active SL structure is similar to those for which evidence of sasing has previously been observed^{40,41}, the higher level of doping used, and hence higher electron density, is such that population inversion throughout the active SL is not achieved under the conditions of the experiment. Therefore the stimulated absorption of phonons is expected to be the dominant process for 378 GHz phonons, and the flux will decrease as we measure experimentally.

The dependence of the relative decrease of α on V , shown on Fig. 4, is an increasing function. It is important that the dependence of α on V is very different from the I - V characteristic of the active SL (see Fig. 1c) thus serving as an additional argument for excluding experimental artefacts, like modulation of sensitivity of the detector by V .

A possible qualitative explanation for the measured dependence of α on V is that, with increasing bias, the electron temperature, T_e , in the active SL increases. The effect of this is to increase the number of possible near-vertical electron transitions involving electron states within a region $\sim kT_e$ of the Fermi energy. This might explain the reasonable fit to the data of a function proportional to the bias dependence of the electrical power dissipated in the active SL. However, for a complete description of the dependence of α on V , a more detailed analysis in respect to the specific model of inhomogeneity and high doping in the studied SL is required, which goes well beyond the scope of the present paper.

Finally, we have performed a phonon optics experiment with the possibility to control the flux of the coherent sub-THz phonons by

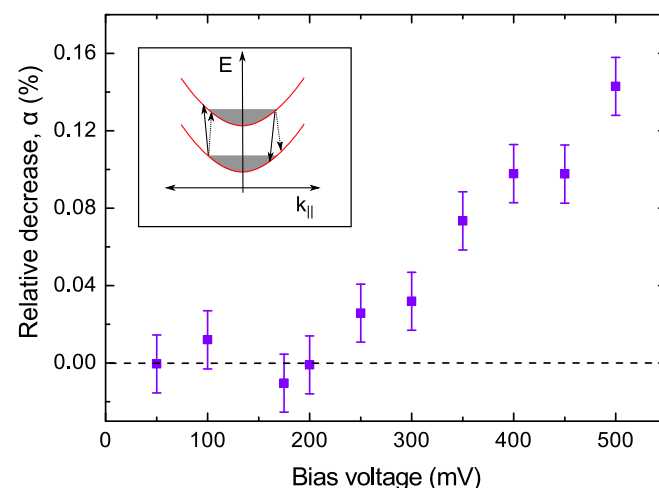


Figure 4 | Electron-Phonon interaction in the active SL. The dependence of the amplitude of the spectral peak at $f_0 = 378$ GHz in bias modulated signal $\Delta P(t)$ on the applied bias V . The inset shows schematically the phonon assisted transitions for electron tunneling between the neighboring GaAs layers in the Stark ladder. Solid and dotted black arrows indicate transitions with absorption or stimulated emission of phonons respectively.



applying external electric field to the doped semiconductor SL inserted in the phononic chip. The layer with the doped SL serves as an active element in the coherent phonon propagation path from the generator to detector. The relative amplitude change of the demonstrated coherent phonon flux modulation has a value $\sim 10^{-3}$, which, although small, was detected with reliable signal to noise level by sensitive detector for coherent phonons based on the p - i - n photodiode. With further work to optimise the structure and doping of the active SL, we believe it should be possible to increase the depth of modulation. Phononic chips with coherent detectors and generators separated by a macroscopic distance which can be controlled externally have a potential for exploiting THz and sub-THz acoustics in acousto-electrical, acousto-optical, and thermal devices. It is already believed that coherent phonon optics based on passive devices may cause “Sound and Heat Revolutions in Phononics”²². Inserting active elements in the phononic chips controlled externally will enable much broader possibilities for phonon control on the nanometer scale and related prospective applications.

Methods

Phononic chip. The semiconductor layers in the chip shown in Fig. 1(a) were grown by molecular beam epitaxy (MBE) on both sides of a 164 μm -thick (001) semi insulating GaAs substrate. The active SL consists of 50 periods, each period comprised of 5.9 nm GaAs and 3.9 nm of AlAs, n -doped with Si to a concentration of 10^{17} cm^{-3} . At each end of this are 0.5 μm -thick, electrical contact layers n -doped with Si to a concentration of 10^{18} cm^{-3} . The contact layers are separated from the active SL by 20.2 nm thick GaAs layers in which the doping is linearly graded from 10^{17} to 10^{18} cm^{-3} . On top of the active SL structure, and separated from it by a 100 nm undoped GaAs spacer, is a transducer SL consisting of 50 periods, each of 4 nm GaAs and 11 nm of AlAs. The transducer SL emits a flux of coherent phonons when excited by a femtosecond laser pulse with a photon energy greater than the lowest energy of electron-hole resonance in the GaAs layers, 1.76 eV in this case. The calculated frequency of the dominant phonon mode in the phonon flux is given by $f_0 \approx cd_{\text{SL}} = 380 \text{ GHz}$ (c is the speed of longitudinal sound in the SL and d_{SL} is the SL period), which is well away from the phononic stop bands of the active SL. The phonon detector based on the p - i - n photodiode was grown by MBE on the opposite side of the substrate. The phonon detector consists of 3 period SL with 1.2 nm of GaAs and 1 nm of $\text{Al}_{0.33}\text{Ga}_{0.77}\text{As}$. It is grown in the middle of a 200 nm-thick undoped (i -intrinsic) $\text{Al}_{0.33}\text{Ga}_{0.77}\text{As}$ layer and has maximum sensitivity to phonons when probed with the optical pulses with photon energy $\sim 1.76 \text{ eV}$, close to the band gap of GaAs layers in the SL. The i -region is embedded between 200 nm thick contacts from n -doped (10^{18} cm^{-3} Si) $\text{Al}_{0.33}\text{Ga}_{0.77}\text{As}$ and p -doped (10^{18} cm^{-3} C) $\text{Al}_{0.33}\text{Ga}_{0.77}\text{As}$ layers. This particular structure was chosen so that its optical resonance matched the optical resonance of the phonon transducer SL, and it was found to be at least as sensitive as the single GaAs quantum well based structure⁴².

Pumping and probing the phonon signal. Optical pump and probe beams came from a tuneable mode locked Ti:sapphire $\sim 100 \text{ fs}$ pulsed laser with a repetition frequency of 82 MHz operating at a wavelength of 700 nm. After passing through the motorized optical delay line the pump beam was focused on the transducer SL to the 50 μm diameter spot and the maximum energy density at the surface of the phononic chip was $\sim 50 \text{ J/cm}^2$ per pulse. The probe beam was focused on the p - i - n detector to the spot with diameter $\sim 20 \text{ }\mu\text{m}$. The amplified photocurrent of the biased p - i - n was detected by the lock-in amplifier referenced to 15 kHz from the acousto-optical modulator in the path of the pump beam (in experiments with $V = 0$) or from the pulses controlling the bias modulation in the active SL.

Generation of strain pulses at the interfaces in the phononic chip. The signal $P_0(t)$ shows a number of sharp peaks. Three of them are explained in the caption of Fig. 2 and the related text. The temporal shape $P_0(t)$ also possesses other peaks with smaller amplitudes which may be explained by the arrival of the strain pulses generated at various interfaces due to stress induced by optical pump excitation. The total number of peaks also includes the echoes in the p - i - n diode due to the phonon reflection at the open surface from the side of phonon detector⁴². All these peaks form the lower frequency part of the phonon spectrum detected by the p - i - n photodiode and shown in Fig. 2 (b) and do not influence the conclusions of the present work.

Analysis. We checked experimentally measuring $P_V(t)$ applying dc bias V (without bias modulation) that $\Delta A/A$ and $2\pi f_0 \Delta t$ are both much less than unity. We may get the following equation for the ratio α :

$$\alpha = \sqrt{(\Delta A/A_0)^2 + (2\pi f_0 \Delta t)^2}. \quad (1)$$

When $\Delta t = 0$ (no bias induced changes in the arrival time), then $\alpha = |\Delta A/A_0|$ and the phase shift $\Delta\Psi = 0$ or $\Delta\Psi = \pi$ when the applied bias induces the increase or the decrease of the amplitude of harmonic oscillations respectively. In the other extreme

case, when $\Delta A = 0$, $\alpha = |2\pi f_0 \Delta t|$ and $\Delta\Psi = \pm \pi/2$. In more the general case, $\Delta t \neq 0$ and $\Delta A \neq 0$, the phase difference is equal to:

$$\Delta\Psi = (H(\Delta A) - 1)\pi + \arctan\left(\frac{2\pi f_0 A_0 \Delta t}{\Delta A}\right), \quad (2)$$

where $H(x)$ is the Heaviside function. Eq.(2) allows one to conclude that the experimentally measured value $\Delta\Psi = 0.76\pi$ may be realized only if $\Delta A < 0$ and this means a decrease of the oscillation amplitude when bias is applied to the active SL. Using the experimentally measured value of $\Delta\Psi$ and Eq.(2) we may estimate Δt . Following this Eq.(1) and the experimentally measured value of α may be used to estimate $(\Delta A/A_0)$.

- Young, E. S. K., Akimov, A. V., Henini, M., Eaves, L. & Kent, A. J. Subterahertz Acoustical Pumping of Electronic Charge in a Resonant Tunneling Device. *Phys. Rev. Lett.* **108**, 226601 (2012).
- Moss, D. M., Akimov, A. V., Glavin, B. A., Henini, M. & Kent, A. J. Ultrafast strain-induced current in a GaAs Schottky diode. *Phys. Rev. Lett.* **106**, 066602 (2011).
- Lanzillotti-Kimura, N. D., Fainstein, A., Lemaître, A., Jusserand, B. & Perrin, B. Coherent control of sub-terahertz confined acoustic nanowaves: Theory and experiments. *Phys. Rev. B* **84**, 115453 (2011).
- Li, N. *et al.* Colloquium: Phononics: Manipulating heat flow with electronic analogs and beyond. *Rev. Mod. Phys.* **84**, 1045 (2012).
- Gadalla, A., Dehoux, T. & Audoin, B. Transverse mechanical properties of cell walls of single living plant cells probed by laser-generated acoustic waves. *Planta* **239**, 1129-1137 (2014).
- Dehoux, T. & Audoin, B. Non-invasive optoacoustic probing of the density and stiffness of single biological cells. *J. Appl. Phys.* **112**, 124702 (2012).
- Wang, L. V. & Hu, S. Photoacoustic tomography: in vivo imaging from organelles to organs. *Science* **335**, 1458-1462 (2012).
- Dehoux, T., Wright, O. B., Voti, R. L. & Gusev, V. E. Nanoscale mechanical contacts probed with ultrashort acoustic and thermal waves. *Phys. Rev. B* **80**, 235409 (2009).
- Ristow, O. *et al.* Ultrafast spectroscopy of super high frequency mechanical modes of doubly clamped beams. *Appl. Phys. Lett.* **103**, 233114 (2013).
- Cuffe, J. *et al.* Lifetimes of confined acoustic phonons in ultrathin silicon membranes. *Phys. Rev. Lett.* **110**, 095503 (2013).
- Poliani, E. *et al.* Nanoscale imaging of InN segregation and polymorphism in single vertically aligned InGaN/GaN multi quantum well nanorods by tip-enhanced Raman scattering. *Nano Lett.* **13**, 3205-3212 (2013).
- Graczykowski, B. *et al.* Acoustic phonon propagation in ultra-thin Si membranes under biaxial stress field. *New J. Phys.* **16**, 073024 (2014).
- Lin, K.-H. *et al.* Spatial manipulation of nanoacoustic waves with nanoscale spot sizes. *Nat Nanotechnol* **2**, 704-708 (2007).
- Abi Ghanem, M. *et al.* Remote opto-acoustic probing of single-cell adhesion on metallic surfaces. *J. biophotonics* **7**, 453-459 (2014).
- Dehoux, T. *et al.* Probing single-cell mechanics with picosecond ultrasonics. *Ultrasonics* (2014).
- Scherbakov, A. V. *et al.* Ultrafast control of light emission from a quantum-well semiconductor microcavity using picosecond strain pulses. *Phys. Rev. B* **78**, 241302 (2008).
- Brüggemann, C. *et al.* Laser mode feeding by shaking quantum dots in a planar microcavity. *Nature Photon* **6**, 30-34 (2012).
- Jäger, J. V. *et al.* Picosecond inverse magnetostriction in galphenol thin films. *Appl. Phys. Lett.* **103**, 032409 (2013).
- Bombeck, M. *et al.* Magnetization precession induced by quasitransverse picosecond strain pulses in (311) ferromagnetic (Ga, Mn) As. *Phys. Rev. B* **87**, 060302 (2013).
- Bruchhausen, A. *et al.* Investigation of coherent acoustic phonons in terahertz quantum cascade laser structures using femtosecond pump-probe spectroscopy. *J. Appl. Phys.* **112**, 033517 (2012).
- Pascual-Winter, M. F., Fainstein, A., Jusserand, B., Perrin, B. & Lemaître, A. Spectral responses of phonon optical generation and detection in superlattices. *Phys. Rev. B* **85**, 235443 (2012).
- Maldovan, M. Sound and heat revolutions in phononics. *Nature* **503**, 209-217 (2013).
- Narayanaamurti, V. Phonon optics and phonon propagation in semiconductors. *Science* **213**, 717-723 (1981).
- Von Gutfeld, R. J. Heat pulse transmission. in *Physical Acoustics: Principles and Methods*, vol. 5, Ed. Warren P. Mason (Academic Press, New York, 1986).
- Dynes, R. C., Narayanaamurti, V. & Chin, M. Monochromatic phonon propagation in Ge: Sb using superconducting tunnel junctions. *Phys. rev. Lett.* **26**, 181 (1971).
- Eisenmenger, W. & Kaplyanskii, A. A. Nonequilibrium phonons in nonmetallic crystals. (*Modern Problems in Condensed Matter Science*, vol. 16), (Elsevier Science Ltd, Amsterdam: North Holland, 1986).
- Grahn, H. T., Maris, H. J. & Tauc, J. Picosecond ultrasonics. *IEEE J. Quant. Electron* **25**, 2562-2569 (1989).
- Maris, H. J. Picosecond ultrasonics. *Sci. Am.* **278**, 86-89 (1998).
- Baumberg, J. J., Williams, D. A. & Köhler, K. Ultrafast acoustic phonon ballistics in semiconductor heterostructures. *Phys. Rev. Lett.* **78**, 3358 (1997).



30. Daly, B. C. *et al.* Imaging nanostructures with coherent phonon pulses. *Appl. Phys. Lett.* **84**, 5180-5182 (2004).
31. Dehoux, T., Wright, O. B. & Voti, R. L. Picosecond time scale imaging of mechanical contacts. *Ultrasonics* **50**, 197-201 (2010).
32. Tas, G. *et al.* Noninvasive picosecond ultrasonic detection of ultrathin interfacial layers: CFx at the Al/Si interface. *Appl. Phys. Lett.* **61**, 1787-1789 (1992).
33. Chen, H.-P. *et al.* Femtosecond laser-ultrasonic investigation of plasmonic fields on the metal/gallium nitride interface. *Appl. Phys. Lett.* **97**, 201102 (2010).
34. Salasyuk, A. S. *et al.* Filtering of elastic waves by opal-based hypersonic crystal. *Nano Lett.* **10**, 1319-1323 (2010).
35. Lanzillotti-Kimura, N. D., Fainstein, A., Balseiro, C. A. & Jusserand, B. Phonon engineering with acoustic nanocavities: Theoretical considerations on phonon molecules, band structures, and acoustic Bloch oscillations. *Phys. Rev. B* **75**, 024301 (2007).
36. Chen, W., Lu, Y., Maris, H. J. & Xiao, G. Picosecond ultrasonic study of localized phonon surface modes in Al/Ag superlattices. *Phys. Rev. B* **50**, 14506 (1994).
37. Schneider, D. *et al.* Defect-controlled hypersound propagation in hybrid superlattices. *Phys. Rev. Lett.* **111**, 164301 (2013).
38. Kent, A. J. *et al.* Acoustic phonon emission from a weakly coupled superlattice under vertical electron transport: observation of phonon resonance. *Phys. Rev. Lett.* **96**, 215504 (2006).
39. Beardsley, R. P., Akimov, A. V., Henini, M. & Kent, A. J. Coherent terahertz sound amplification and spectral line narrowing in a stark ladder superlattice. *Phys. Rev. Lett.* **104**, 085501 (2010).
40. Maryam, W., Akimov, A. V., Campion, R. P. & Kent, A. J. Dynamics of a vertical cavity quantum cascade phonon laser structure. *Nat. Comm.* **4** (2013).
41. Beardsley, R. P., Campion, R. P., Glavin, B. A. & Kent, A. J. A GaAs/AlAs superlattice as an electrically pumped THz acoustic phonon amplifier. *New J. Phys.* **13**, 073007 (2011).
42. Moss, D. *et al.* Picosecond strain pulses probed by the photocurrent in semiconductor devices with quantum wells. *Phys. Rev. B* **83**, 245303 (2011).
43. Bonilla, L. L. & Grahn, H. T. Non-linear dynamics of semiconductor superlattices. *Rep. Prog. Phys.* **68**, 577 (2005).
44. Bartels, A., Dekorsy, T., Kurz, H. & Köhler, K. Coherent zone-folded longitudinal acoustic phonons in semiconductor superlattices: excitation and detection. *Phys. Rev. Lett.* **82**, 1044 (1999).
45. Winter, M. P., Fainstein, A., Jusserand, B., Perrin, B. & Lemaître, A. Optimized optical generation and detection of superlattice acoustic phonons. *Appl. Phys. Lett.* **94**, 103103 (2009).
46. Cottam, R. I. & Saunders, G. A. The elastic constants of GaAs from 2 K to 320 K. *J. Phys. C* **6**, 2105 (1973).
47. Adachi, S. *Handbook on physical properties of semiconductors*. Vol. 2 (Kluwer Academic publishers, USA, 2004).
48. Chen, W., Maris, H. J., Wasilewski, Z. R. & Tamura, S.-I. Attenuation and velocity of 56 GHz longitudinal phonons in gallium arsenide from 50 to 300 K. *Philos. Mag. B* **70**, 687-698 (1994).
49. Grahn, H. T. *Semiconductor superlattices: growth and electronic properties*. (World Scientific Publishing Co., Singapore 1995).
50. Kent, A. J. & Wigmore, J. K. Energy relaxation by hot 2D carriers. in *Electron-Phonon Interactions in Low-Dimensional Structures*. Ed. Lawrence Challis (Oxford University Press, Oxford, 2003).
51. Glavin, B. A., Kochelap, V. A., Linnik, T. L., Kim, K. W. & Stroschio, M. A. Generation of high-frequency coherent acoustic phonons in superlattices under hopping transport. I. Linear theory of phonon instability. *Phys. Rev. B* **65**, 085303 (2002).

Acknowledgments

The authors acknowledge support for this work from DARPA under the European Office of Aerospace Research and Development contract no. FA8655-13-1-2046. The authors also acknowledge helpful discussions with Boris Glavin (ISP - Kiev) relating to some of the theoretical aspects of the work.

Author contributions

A.J.K. and A.V.A. developed the idea for the experiment, C.L.P. and A.V.A. performed the experiment, C.L.P., A.V.A. and A.J.K. analysed the experimental data and wrote the manuscript, R.P.C. fabricated the samples.

Additional information

Competing financial interests: The authors declare no competing financial interests.

How to cite this article: Poyser, C.L., Akimov, A.V., Campion, R.P. & Kent, A.J. Coherent phonon optics in a chip with an electrically controlled active device. *Sci. Rep.* **5**, 8279; DOI:10.1038/srep08279 (2015).



This work is licensed under a Creative Commons Attribution 4.0 International License. The images or other third party material in this article are included in the article's Creative Commons license, unless indicated otherwise in the credit line; if the material is not included under the Creative Commons license, users will need to obtain permission from the license holder in order to reproduce the material. To view a copy of this license, visit <http://creativecommons.org/licenses/by/4.0/>